JACS
JOURNAL OF THE AMERICAN CHEMICAL SOCIETY
Article
pubs.acs.org/JACS

# Colloidal Lock-and-Key Dimerization Reactions of Hard Annular Sector Particles Controlled by Osmotic Pressure

Po-Yuan Wang[†] and Thomas G. Mason*[,‡,§]

[†]Department of Materials Science and Engineering, [‡]Department of Chemistry and Biochemistry, and [§]Department of Physics and Astronomy, University of California—Los Angeles, Los Angeles, California 90095, United States

**ABSTRACT:** Colloidal annular sectors are a broad class of shapes that offer the interesting possibility of dimerization when osmotically compressed to high densities while undergoing Brownian motion in two dimensions (2D). Here, we lithographically create and form a stable aqueous dispersion of many microscale prismatic 270° annular sectors, and we explore their near-equilibrium behavior in a tilted 2D gravitational column. Near the top of the column where the 2D gravitational osmotic pressure $\Pi_{2D}$ is low, we observe a gas-like phase composed almost entirely of monomers. However, below the surface and deeper into the column where $\Pi_{2D}$ is higher, we observe a reaction zone where monomers and dimers coexist, followed by an arrested region containing a very high percentage of interpenetrating, lock-and-key dimers that are a racemic mixture of positive and negative chiralities. We determine particle area fractions of monomers and dimers as a function of depth and use these to obtain the system's 2D osmotic equation of state. In the reaction zone, where dimers transiently form and break up, we also use these to calculate the equilibrium constant $K$ associated with the monomer−dimer reaction, which increases exponentially with $\Pi_{2D}$. This dependence can be attributed the reduction in number of accessible microstates for dimers as they become more tightly compressed.

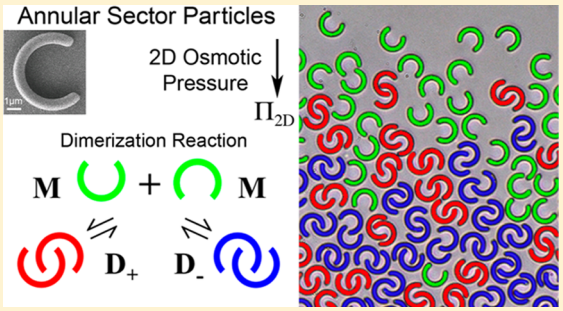


## INTRODUCTION

The simplest structure that can be assembled out of two identical monomer building blocks is the dimer. A wide variety of dimers occur naturally at everyday conditions. Certain diatomic molecules, such as oxygen $O_2$ and nitrogen $N_2$,[1] are homodimers made of atomic building blocks, whereas dimers of capsid coat proteins, such as those of simple bromoviruses,[2,3] can themselves serve as more complex building blocks for other supramolecular structures. Many different mechanisms can play a role in dimer formation. For instance, electronic and quantum mechanical pair interactions between monomer atoms can lead to diatomic molecule formation through strong attractions associated with covalent bonding. Alternatively, entropically driven anisotropic roughness-controlled depletion attractions (RCDAs)[4,5] between plate-like colloids,[6] each of which has a rougher face and a smoother face, can be used to form a stable phase of dimers: the smoother faces of two platelets are attractively bound together inside each dimer and the outer surfaces of each dimer are entirely rough, thereby precluding subsequent aggregation.[7] Through a different mechanism, hydrogen bonding can cause self-association of two molecules of acetic acid in certain organic solvents, yielding linear and cyclic dimers.[8] As yet a different example, certain localized site-specific attractive and repulsive interactions between two proximate monomer protein molecules can also lead to dimer formation, yielding highly reproducible dimer protein structures.[9−14] Often, the core shapes of these molecules have convex protrusions and also concave receptacles, enabling mutually interpenetrating lock-and-key dimer structures to be assembled.

The formation reaction of two monomer building blocks into a dimer is known as a dimerization reaction, and the decomposition reaction of a dimer into two separate monomers is called a dissociation or a dedimerization reaction. If the two monomers are identical, then the reaction is a homodimerization reaction. For systems composed of many monomers, in which attractive interactions between monomers are the mechanism for dimer formation, the proportions of monomers and dimers in equilibrium at a certain temperature $T$ and a pressure $p$ are well-known. The equilibrium reaction between two monomers has a forward dimerization rate constant $k_+$ and also a backward dissociation rate constant $k_-$, where the equilibrium constant $K$ of the reaction is simply $K = k_+/k_-$.[8] In cases when attractive interactions between monomers drive dimerization, if the pair attraction has an effective bond energy, $U$, (e.g., associated with a minimum in a potential well), then dimers will dominate when $U$ is much larger than thermal energy $k_BT$. However, if the temperature is raised so that $k_BT$ becomes much larger than $U$, then monomers will dominate.[7] For many attractive monomer−dimer systems, pressure typically only plays a secondary role.

While equilibrium dimerization and dimer dissociation reactions for attractive monomer building blocks are well-known, regardless of whether or not the two building blocks

**Received:** October 8, 2015
**Published:** November 24, 2015





DOI: 10.1021/jacs.5b10549
J. Am. Chem. Soc. 2015, 137, 15308−15314

mutually interpenetrate to form lock-and-key structures, much less is known about dimerization of systems of shapes at equilibrium in which pair interactions are effectively hard, so that only geometrical shape of the monomer and entropy at a certain pressure and temperature control the degree of dimerization. Moreover, the meaning of dimerization must somehow be defined geometrically for such systems of hard shapes, and the requirement of mutual interpenetration of two monomer shapes into a single lock-and-key dimer structure could be used as this definition. Unanswered questions exist about the range and types of monomer shapes that could lead to significant populations of dimer structures when Brownian systems of monomers are slowly concentrated to high densities. Particularly, in colloidal systems of solid particles dispersed in a weakly viscous liquid, the advent of shape-designed platelets[15−18] and the creation of two-dimensional (2D) near-equilibrium systems of these shapes over a wide range of particle densities[19,20] offers the potential for exploring the behavior of hard shapes that could potentially dimerize into interpenetrating lock-and-key structures. For such 2D colloidal systems, one would expect that $K$ of the dimerization reaction would depend on the 2D osmotic pressure, $\Pi_{2D}$, since $\Pi_{2D}$ is related to the area fraction of particles, $\phi_A$, through an osmotic equation of state $\Pi_{2D}(\phi_A)$.[21] Even having a single robust experimental demonstration of the behavior of a lock-and-key colloidal dimerization reaction over a wide range of applied $\Pi_{2D}$ in a thermally excited system would represent an important advance in understanding the fundamental behavior of colloidal dimerization of hard objects.

RCDAs have been demonstrated to provide a robust route for forming 2D Brownian systems of lithographic platelets, thereby enabling experimental exploration of the phase behavior of dense systems having a wide variety of shapes over a range of particle area fractions $\phi_A$. RCDAs keep microscale platelets oriented with their faces parallel to a transparent, solid, smooth substrate, yet in-plane interactions remain effectively hard. Many particles in a plane are then concentrated very slowly by tilting the substrate (e.g., a sealed rectangular cuvette) by a small angle, so that gravitational sedimentation of the platelets effectively applies a two-dimensional osmotic pressure that varies with the distance along the substrate.[19]

While 2D Brownian systems of hard shapes explored experimentally thus far have been mostly convex polygons, such as triangles,[22] squares,[20] pentagons,[19] rhombs,[23] parallelograms,[24] and kites,[25] some other shapes have had forms of concavity, including arms. Four-arm square crosses have been shown to form chiral crystallites at high densities,[26] whereas slender three-arm tristar particles form large crystallites of an alternating stripe crystal, reminiscent of steric zippers.[21] These shapes have yielded a wide variety of self-organized structures, yet thus far, topologically identifiable lock-and-key dimerization in dense Brownian systems of colloidal objects that have hard interactions has not been explored experimentally.

In order for two copies of a single, hard, monomer shape to have the possibility of forming a lock-and-key dimer, that monomer shape must necessarily possess both a concave portion and also a convex portion. One of the simplest shapes in 2D that satisfies this requirement is the annular sector.[27] An annular sector has a perimeter given by four segments: an outer arc that has a radius $R_o$ and a filled angle of $2\pi - \psi$, an inner arc that has a radius $R_i$ and the same filled angle $2\pi - \psi$, and two radial line segments of length $\Delta R = R_o - R_i$ connecting the inner arc to the outer arc. Thus, the opening angle that is not filled is $\psi$, and the annular sector's in-plane radial width is $\Delta R$. Annular sectors represent an interesting class of shapes encompassing structures ranging from nearly rectangular to pie-like to nearly toroidal (i.e., ring-like). For $0 < \psi < 2\pi$, an annular sector necessarily has a concave feature (i.e. the inner circular arc) as part of its perimeter; the convex portions consist of the outer arc, as well as the ends of two arms that are terminated by the radial line segments. If $R_o$ and $R_i$ are both greater than $\Delta R$ and $\psi R_i$ is also at least somewhat larger than $\Delta R$, then the ends of the arms will have a significantly larger convex curvature than the concave curvature and one of these arms of a first annular sector can potentially insert reversibly into the opening of a second neighboring annular sector, yielding a lock-and-key dimer configuration. Thus, we design open ring-like microscale platelets that meet these requirements and refer to them as annular sector particles (ASPs). In particular, we focus on ASPs having $\psi \approx \pi/2$, $R_o \approx 3$ $\mu$m, and $\Delta R \approx 1$ $\mu$m, since this partial ring has an opening angle that offers good potential for dimerization. The size of the ASPs, set by $R_o$, is small enough that their Brownian motion is significant, yet large enough that they can be easily observed using an optical microscope.

Here, we show that 2D Brownian systems of designer microscale lithographic ASPs, when slowly compressed osmotically in 2D to large enough $\Pi_{2D}$, can dimerize at an efficiency nearing 100%. Moreover, below a predominantly monomer fluid zone, in the tilted cell of ASPs, we demonstrate that there is a near-surface equilibrium reaction zone. In this spatially resolved reaction zone, dimerization and dedimerization reactions both occur, so we are able to use particle counting statistics to directly determine how the degree of dimerization, given by the equilibrium constant $K$, depends on $\Pi_{2D}$. In addition, we reveal the presence of two distinguishably different positive and negative chiralities of dimers in racemic proportions, and show that the spatial pair correlation function, based on the center positions of ASPs, contains a prominent dimer peak as well as two other peaks that are effectively related to the dimensions of the oblique two-ASP dimer unit.

## EXPERIMENTAL SECTION

Using top-down photolithography (ASML stepper, PAS 5500/200, 5X reduction, ultraviolet (UV) i-line 365 nm), we fabricate microscale plate-like ASPs composed of cross-linked SU-8 polymer photoresist.[15] Into this stepper, we load a negative quartz-chrome mask (MEBES, electron beam lithography, 50 nm feature size) that has been designed (L-Edit, Tanner Research, Inc.) with a rectangular array of annular sector shapes having an opening angle of $\psi = 90.0°$, an inner radius of 15.4 $\mu$m, and an outer radius of 10.2 $\mu$m, as shown in Figure 1a. We prepare a water-soluble sacrificial layer on 4-in. silicon wafers by spin-coating LOR-1A (Microchem Inc.), yielding a thickness $\approx$ 120 nm after baking at 200 °C for 120 s and cooling to room temperature. On the layer of LOR-1A, we spin coat SU-8-2001 (Microchem Inc.) photoresist, which is baked at 95 °C for 90 s, yielding a 1 $\mu$m uniform SU-8 layer. A coated wafer is loaded into the stepper, exposed to patterned UV light, postbaked, and developed in order to remove unexposed and un-cross-linked SU-8. After developing, this wafer is rinsed with isopropyl alcohol and dried with a flow of nitrogen gas, leaving prismatic annular sector particles composed of SU-8 attached to the sacrificial layer of LOR-1A. This sacrificial layer is then dissolved in a basic surfactant solution containing 1.8% w/v tetramethylammonium hydroxide (TMAH, Sigma-Aldrich, 25% in water) and 40 mM sodium dodecyl sulfate (SDS, MP ultrapure), and the particles lift-off into the solution. The hydrophobic tails of SDS molecules adsorb on the surfaces of the SU-8 particles, providing a high enough surface


DOI: 10.1021/jacs.5b10549
J. Am. Chem. Soc. 2015, 137, 15308−15314

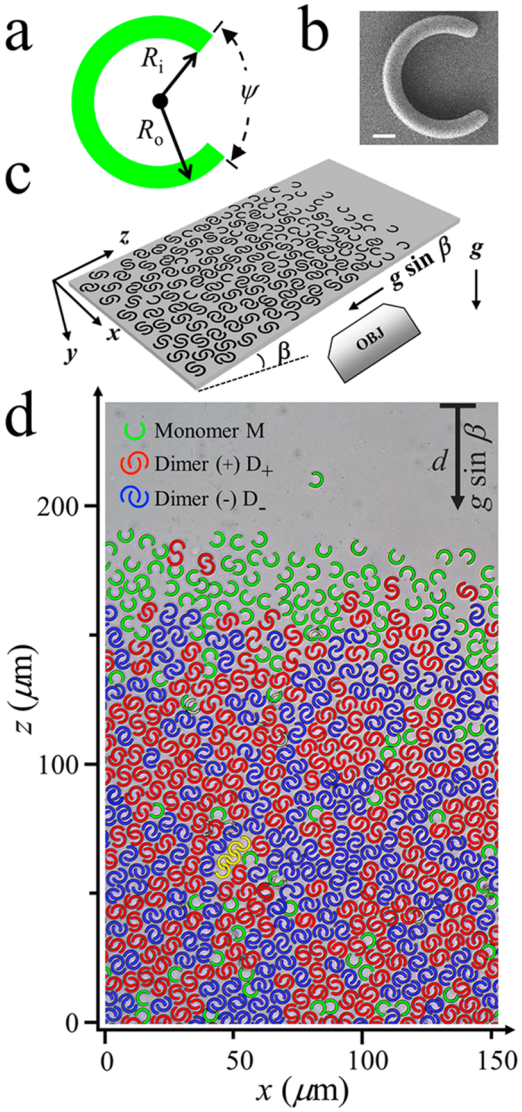


**Figure 1.** Brownian microscale annular sector particles (ASPs), confined to a plane above the lower glass wall of a tilted optical cell, self-organize while diffusing in the presence of a gravitational osmotic pressure. (a) Schematic of an ASP as designed: $R_i$, $R_o$, and $\psi$ are its inner radius, outer radius, and opening angle, respectively. The black dot is the common center of the inner and outer circular arcs. (b) Scanning electron micrograph of a lithographically fabricated annular sector (scale bar: 1 $\mu$m). (c) Schematic of a tilted 2D gravitational column of annular sectors after settling and equilibrating near one end of the optical cell. The tilt angle is $\beta$. OBJ: optical microscope's objective lens (40×, extra long working distance). (d) Grayscale brightfield transmission optical micrograph after equilibration at $\beta = 5$ deg over 3 months. The depth into the gravitational column is $d$. Each ASP has been color-coded via postacquisition digital analysis: monomer M (green), dimer(+) $D_+$ (red), dimer(−) $D_-$ (blue), and chain (yellow). Inset (upper left): visual legend defining M, $D^+$, and $D^-$.

charge to stabilize the particles against aggregation. By successively concentrating the dispersion, removing the supernatant, and diluting it four times in aqueous solutions of deionized water at 5 mM SDS, we remove any residual dissolved LOR-1A and TMAH, and we also set [SDS] = 5 mM. By processing three wafers and combining the results after washing, we obtain an aqueous dispersion containing ≈300 million stabilized ASPs at [SDS] = 5 mM.

We use scanning electron microscopy (SEM), rather than optical microscopy, to characterize the dimensions and shapes of the ASPs precisely, since optical diffraction smears out submicron features. In Figure 1b, we show the face-on view of a typical SU-8 ASP, obtained using JEOL, JSM-6700 FE-SEM, 5 kV. By performing SEM on 10 different particles, we determine the average outer radius to be $R_o$ = 2.8 ± 0.1 $\mu$m and the average inner radius to be $R_i$ = 2.1 ± 0.1 $\mu$m, near the designed values that are 5x smaller than the mask radii, yielding a facial particle area of $A_p$ = 10.0 ± 0.2 $\mu m^2$. SEM side-views reveal a thickness of 1.0 ± 0.1 $\mu$m. The measured average opening angle is $\psi = 95° \pm 1°$, somewhat larger than designed. Optical diffraction also rounds the corners of the fabricated ASPs (radius of curvature for rounding ≈200 nm)[20] and causes the measured $\psi$ to be somewhat larger than designed.

To form the 2D system, we mix a dilute dispersion of stabilized ASPs with a dispersion of a depletion agent composed of 42 nm diameter polystyrene (PS) spheres (carboxylate stabilized, surfactant free), yielding a final postmixing ASP volume fraction of $\phi \approx 0.03\%$, volume fraction of depletion agent $\phi_d \approx 0.5\%$, and [SDS] = 5 mM.[19,20] From the resulting mixed dispersion, a portion containing ≈$10^5$ ASPs is loaded into a rectangular microcuvette (30 mm × 2.0 mm × 0.1 mm) and sealed using UV optical adhesive (Norland type 81). The diameter of the depletion agent has been chosen to lie between the smaller surface roughness on the faces of the ASPs and the larger surface roughness on their sides, thereby making it effective in inducing anisotropic roughness-controlled depletion attractions.[19] We have adjusted $\phi_d$ to provide enough depletion attraction between the glass surface and a flat face of a particle, so that the particles lie flat on the glass substrate, effectively yielding a 2D monolayer of hard, Brownian ASPs. A short-range, Debye-screened electrostatic repulsion, having a screening length of only a few nanometers (i.e., much smaller than the side-roughness of an ASP) caused by adsorbed SDS, also exists between the flat faces of the particles and the lower glass surface, resulting in an aqueous lubricating layer between particles' faces and the proximate surface of the microcuvette. This repulsion also prevents in-plane aggregation of ASPs. Because of the lubricating layer, ASPs diffuse in the monolayer without lifting off or rotating out of the plane, even when a gravitational osmotic pressure is applied by tilting the microcuvette slightly. Because the edges of the ASPs are rougher than their faces, the contact potential associated with the in-plane depletion attraction between two ASPs is less than thermal energy, $k_BT$; thus, ASP pair-interactions are effectively hard.

To explore the emergent self-organization of the 2D Brownian system of annular sectors, we tilt the cuvette along its length by an incline angle of $\beta = 5°$ to gravitationally concentrate the ASPs slowly and quasi-statically over three months, as shown schematically in Figure 1c. After equilibration, annular sectors are imaged at different positions using a Nikon TE2000 inverted microscope equipped with a 40× extra-long working distance objective lens (Nikon Plan Fluor ELWD, 0.6 numerical aperture), and a Nikon D5000 camera (4288 pixels × 2848 pixels). From a digital micrograph, the center coordinates of each annular sector are determined to a precision of about ±100 nm by fitting the outer arc to a circle.

## RESULTS

An optical micrograph of ASPs in an equilibrated 2D column is shown in Figure 1d. We assign a $z$-coordinate that points upward from a reference location in the dense part of column; by contrast, the depth, defined as $d = 240\ \mu m - z$, is measured downward relative to a reference point above all particles, as shown. The total area fraction $\phi_A$ of ASPs increases for larger $d$, ranging from dilute at the top to concentrate toward the bottom. Gravitational forces effectively cause greater compaction of the ASPs deeper into the column, as reflected by the depth-dependent applied osmotic pressure $\Pi_{2D}(d)$. In the dilute region at the top of the column, single ASPs translate and rotate as individual monomers (Ms). However, for larger $d$, $\phi_A$ increases, and some monomers begin to interpenetrate and interlock with neighboring monomers to form dimers, which occupy space more efficiently. In this subsurface region, which


DOI: 10.1021/jacs.5b10549
J. Am. Chem. Soc. 2015, 137, 15308−15314

we refer to as the reaction zone, dimerization and dedimerization reactions occur in equilibrium. If the tip of an arm of one ASP crosses an imaginary line connecting the two tips of the arms of a neighboring ASP, and vice versa, then we consider these two mutually interlocking monomers to form one dimer. In 2D, the dimers are chiral objects, and we classify a dimer as being positive ($D_+$) or negative ($D_-$) according to the two possibilities shown in Figure 1d(inset). In the dense region at large $d$, the annular sectors are predominately in the form of dimers, with the exception of some scattered monomers and a single short chain; these represent defects in the dimer region.

To interpret the osmotic pressure-driven formation of dimers from monomers in this near-equilibrium 2D Brownian system of ASPs quantitatively, we calculate its 2D osmotic equation of state $\Pi_{2D}(\phi_A)$. By filling ASPs in a grayscale micrograph with different colors using Photoshop and counting the colored pixels in a certain local bands (having a $z$-width of about 7.4 $\mu$m), we determine the area fractions of monomers, $\phi_{A,M}$, and all dimers $D_\pm$, $\phi_{A,D\pm}$, as a function of $d$, as shown in Figure 2a.

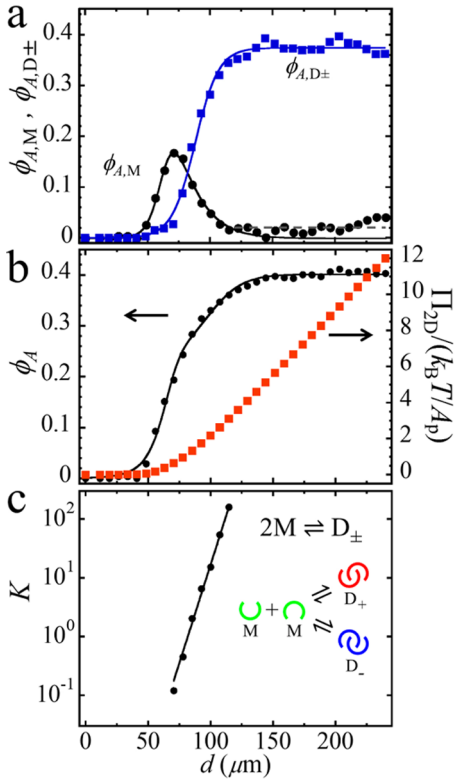


**Figure 2.** Dependence of particle area fraction $\phi_A$, osmotic pressure $\Pi_{2D}$, and equilibrium constant $K$ on the distance $d$ from the top of the tilted 2D column. (a) Area fraction of the monomers ($\phi_{A,M}$, black circles) and dimers ($\phi_{A,D\pm}$, blue squares). Dashed line: average $\phi_{A,M}$ over 125 $\mu$m $\leq d \leq$ 240 $\mu$m. Solid lines: fits to $\phi_{A,M}(d)$ using eq 1 and $\phi_{A,D\pm}(d)$ using eq 2 (see text); these fits intersect at $d^*$ = 81.7 $\mu$m. (b) Total area fraction $\phi_A = \phi_{A,M} + \phi_{A,D\pm}$ (left axis). Solid line: fit by summing eqs 1 and 2. Two-dimensional osmotic pressure $\Pi_{2D}$ calculated from $\phi_A(d)$ by integration, normalized by $k_BT/A_p$, where $T$ is temperature and $A_p$ is the area per particle (right axis). (c) Equilibrium constant $K$, determined from the law of mass action of a monomer−dimer reaction using $\phi_{A,M}$ and $\phi_{A,D\pm}$ as a function of $d$. Here, $K$ = 1 when ASP area fractions of monomers and of dimers are equal (i.e., where $\phi_{A,M} = \phi_{A,D\pm}$ at $d^*$). Solid line: fit using eq 3. Inset: schematic of the equilibrium dimerization reaction: $2M \rightleftharpoons D_\pm$.

In the fluid-like phase at the top of the column, ASPs exist as monomers in the top of column, and a peak in $\phi_{A,M}$ is seen at a location $d_{M,peak} \approx 70$ $\mu$m. Just beyond this peak, $\phi_{A,D\pm}(d)$ increases exponentially and saturates into a plateau at larger $d$. Deep within the column, some scattered single monomers are completely encaged by dimers, and because of crowding, these monomers cannot reach other monomers to combine into dimers through quiescent thermal fluctuations. Consequently, $\phi_{A,M}$ fluctuates around a small value of about 0.02 even in the predominantly dimer region.

The peak in $\phi_{A,M}(d)$ can be empirically fit to a function composed of two exponential factors, each of which has a physical origin. A first factor, $[1 + \exp(-(d - d_{0,M})/h_{g,M})]^{-1}$, describes an initial exponential increase arising from the applied osmotic gravitational pressure, which is given by a barometric law having a thermal-gravitational height for monomers, $h_{g,M}$.[28] A second factor, $[1 + \exp((d - d_{0,M})/L)]^{-1}$, is associated with the exponential reduction of monomers deeper into the column and arises from a pressure-dependent near-equilibrium dimer formation reaction, where $L$ is a characteristic length scale and must be larger than $h_{g,M}$. Here, $d_{0,M}$ is a reference depth near the monomer peak that is common to the two exponential factors. The entire equation can be expressed as

$$\phi_{A,M}(d) = \phi^*_{A,M}\{[1 + \exp(-(d - d_{0,M})/h_{g,M})] [1 + \exp((d - d_{0,M})/L)]\}^{-1} \quad (1)$$

where $\phi^*_{A,M}$ is a scaling prefactor. Fitting the data, we obtain good agreement with a correlation coefficient of 0.93 [Figure 2a]; the fit parameters values are $\phi^*_{A,M} = 0.55 \pm 0.06$, $d_{0,M} = 63 \pm 3$ $\mu$m, $h_{g,M} = 5.6 \pm 1.3$ $\mu$m, and $L = 16 \pm 3$ $\mu$m. The fit agrees very well with the peak, but the fitting function decays to 0 for larger $d$ and is not designed to account for residual trapped monomers within the dimer region where $\phi_{A,M}$ fluctuates around an average of about ≈0.02 [Figure 2a, dashed line].

For dimers, $\phi_{A,D\pm}(d)$ rises rapidly as the monomer concentration is depleted and then effectively saturates at large depths within our measured range. To fit this empirically, only a single factor is needed:

$$\phi_{A,D\pm}(d) = \phi^*_{A,D}[1 + \exp(-(d - d_{0,D})/h_{g,D})]^{-1} \quad (2)$$

where $\phi^*_{A,D}$ describes a plateau value at larger $d$, $d_{0,D}$ is a reference depth for dimers, and $h_{g,D}$ is a characteristic length associated with the conversion of monomers to dimers by the gravitational osmotic pressure, created by particles above the conversion layer. As shown in Figure 2a, a fit using eq 2 to the measured $\phi_{A,D\pm}(d)$ yields excellent agreement (i.e., correlation coefficient = 0.998) and the following parameter values: $\phi^*_{A,D} = 0.370 \pm 0.003$, $d_{0,D} = 88 \pm 1$ $\mu$m, and $h_{g,D} = 9.4 \pm 0.5$ $\mu$m.

The total particle area fraction, $\phi_A(d)$, is shown in Figure 2b and is described by the sum of eqs 1 and 2. We fix $h_{g,M} = 6.9$ $\mu$m and $L = 19$ $\mu$m, using values within about one standard deviation of those obtained by fitting the monomer peak in $\phi_{A,M}(d)$. Because this monomer peak is effectively hidden in the initial rise of $\phi_A(d)$, these parameters cannot be independently extracted by fitting only $\phi_A(d)$ by itself. Fitting $\phi_A(d)$ to the sum yields $\phi^*_{A,M} = 0.44 \pm 0.06$, $d_{0,M} = 68 \pm 1$ $\mu$m, $\phi^*_{A,D} = 0.401 \pm 0.002$, $d_{0,D} = 91 \pm 2$ $\mu$m, and $h_{g,D} = 15 \pm 1$ $\mu$m. These values are in reasonable agreement with those obtained by fitting $\phi_{A,M}(d)$ or $\phi_{A,D\pm}(d)$ separately, within the overlap of standard deviations. Values of $\phi^*_{A,D}$ and $h_{g,D}$ are slightly higher when fitting $\phi_A(d)$; this small systematic deviation can be


DOI: 10.1021/jacs.5b10549
J. Am. Chem. Soc. 2015, 137, 15308−15314

attributed predominantly to the trapped monomer contribution at large $d$ (i.e., the contribution given by the dashed line in Figure 2a) that is not captured in the functional form of eq 1. Overall, all fits to $\phi_{A,M}$, $\phi_{A,D\pm}$, and $\phi_A$ agree well with the measurements, and their parameter values are self-consistent.

Using the measured $\phi_A(d)$, we calculate the applied gravitational 2D osmotic pressure, $\Pi_{2D}$, by summing up the effective buoyant mass of all particles above a particular height $z$: $\Pi_{2D}(z) = (k_BT/A_p)\int_z^\infty \phi_A(z')(dz'/h_{g,M})$, where $z'$ is a variable of integration along the $z$-direction.[21] Here, we have used $h_{g,M} \approx 5.6$ $\mu$m; we estimate that the uncertainty in the overall scale of $\Pi_{2D}$ is about ±25%. After integrating, we convert $z$ to $d$, and we find that $\Pi_{2D}(d)$ begins to rise in the monomer region, and then rises more rapidly at larger $d$ beyond the monomer peak in $\phi_{A,M}(d)$ [Figure 2b, right axis].

Thermal excitations in the Brownian system of ASPs subjected to a slow 2D osmotic compression can lead to dimerization of a pair of neighboring ASPs into a mutually interlocking configuration; a dimer pair can later dedimerize into two monomer ASPs as a consequence of the same thermal excitations. Thus, the transient formation and dissociation of dimers is a dynamic process that is near equilibrium, and we hypothesize that this colloidal equilibrium reaction can be captured by the thermodynamic law of mass action.[1] The chemical equilibrium equation describing dimerization and dedimerization reactions is simply $2M \rightleftharpoons D_\pm$, as illustrated in Figure 2c(inset). The equilibrium constant, $K$, of the dimerization reaction is given by the law of mass action: $K = \phi_{A,D\pm}/\phi_{A,M}^2$. We plot $K$ using the measured $\phi_{A,M}(d)$ and $\phi_{A,D\pm}(d)$, and we choose $K = 1$ where $\phi_{A,M} = \phi_{A,D\pm}$, at $d^* = 81.7$ $\mu$m, as determined by interpolation [Figure 2c]. Below the dilute surface fluid of monomers, in the active monomer−dimer reaction layer given by 70 $\mu$m < $d$ < 125 $\mu$m, $K(d)$ increases exponentially and can be fit well to

$$K = \exp[(d - d^*)/L_D] \quad (3)$$

where $L_D = 6.49 \pm 0.01$ $\mu$m is a characteristic entropic-osmotic length scale associated with dimer formation. The exponential growth in $K$ shows that neighboring monomer ASPs efficiently convert into local dimer configurations when the applied osmotic compression begins to approach and exceed $\Pi_{2D}(d^*) \approx 2k_BT/A_p$.

The 2D osmotic equation of state, $\Pi_{2D}(\phi_A)$, of ASPs is calculated by eliminating the common parameter $d$ in $\phi_A(d)$ and $\Pi_{2D}(d)$, and normalized by the 2D thermal energy density $k_BT/A_p$ as shown in Figure 3a. Over a wide range of $\phi_A$, the scaled 2D osmotic equation of state can be fit to the semiempirical form describing a crossover from an ideal-gas law to a jamming divergence:[21]

$$\Pi_{2D}(\phi_A)/(k_BT/A_p) = f\phi_A/[1 - (\phi_A/\phi_{A,c})] \quad (4)$$

where $f$ is a dimensionless prefactor and $\phi_{A,c}$ is a critical area fraction, corresponding to a divergence in $\Pi_{2D}$ at a jamming point. The fit accurately describes the data up to $\phi_A \approx 0.38$, yielding $f = 1.79 \pm 0.03$ and $\phi_{A,c} \approx 0.455 \pm 0.001$. For reference, an ideal gas of point-like particles would have $f = 1$; ASPs are not point-like, so a value of $f$ near unity is reasonable. Interestingly, the 2D osmotic equation of state does not reveal any abrupt features, which could possibly result from the underlying dimerization reaction, so the progression from predominately monomers to predominately dimers is gradual.

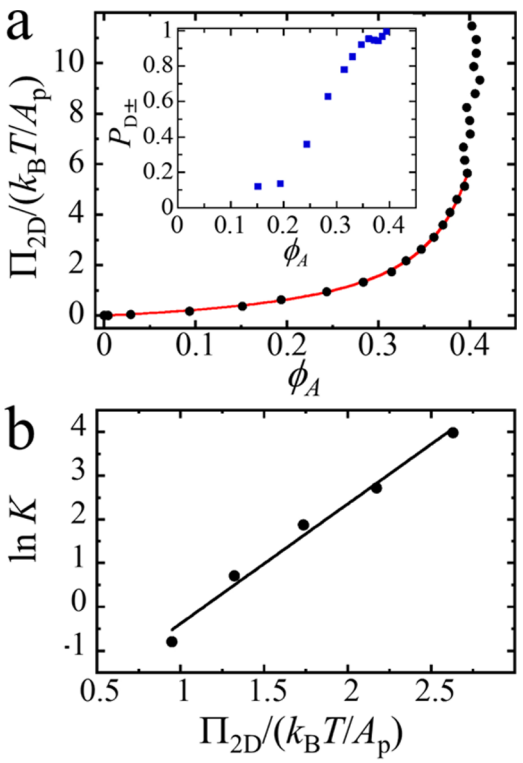


**Figure 3.** (a) Osmotic equation of state of ASPs, given by the scaled 2D osmotic pressure $\Pi_{2D}/(k_BT/A_p)$ as a function of total particle area fraction $\phi_A$. Solid red line: fit to $f\phi_A/[1 - (\phi_A/\phi_{A,c})]$; see text. Inset: probability of dimerization, $P_{D\pm}$, as a function of $\phi_A$. (b) Equilibrium constant $K$ increases exponentially as a function of $\Pi_{2D}/(k_BT/A_p)$. Solid line: linear fit to ln $K$ vs $\Pi_{2D}/(k_BT/A_p)$, yielding a slope of 2.7 ± 0.2.

We also express the measured probability, $P_{D\pm}$, of an ASP being found in a dimer configuration as a function of $\phi_A$ [see Figure 3a inset]. For $\phi_A$ < 0.2, toward the dilute limit, the system is predominantly populated by monomers: $P_{D\pm} < 0.1$. However, in the monomer−dimer reaction zone, for 0.2 < $\phi_A$ < 0.3, monomers and dimers coexist in different proportions and $0.1 \le P_{D\pm} \le 0.9$. In the highly concentrated regime for $\phi_A$ > 0.3, long-lived dimers predominate $P_{D\pm} > 0.9$, yet a small fraction of monomers remain; these are typically isolated from other monomers, so they cannot react and therefore are trapped.

The intrinsic nature of the pressure-driven dimerization reaction in the Brownian system of hard ASPs can be seen most obviously by plotting the natural logarithm of the dimerization equilibrium constant, ln $K$ versus $\Pi_{2D}/(k_BT/A_p)$ [see Figure 3b], where data have been limited to the monomer−dimer reaction zone. A linear fit provides good agreement and yields a slope of 2.7 ± 0.2, implying that the number of accessible monomer microstates dramatically decreases as the applied $\Pi_{2D}$ is raised near and above the entropic level $(k_BT/A_p)$.

In order to characterize the structure of ASPs at high density in the dimer region, we calculate the spatial pair correlation function $g(r/D_o)$,[28,29] where $r$ is the separation between centers of two ASPs and $D_o = 2R_o$ is the outer diameter of an ASP, for 0 $\mu$m ≤ $z$ ≤ 88 $\mu$m, as shown in Figure 4a. Interestingly, $g(r/D_o)$ shows a strong discrete peak located at an unusually small value of $r/D_o \approx 0.32$, signaling the interpenetration of the ASPs that are dimerized as either $D_+$ or $D_-$. Thus, we define $r_d \approx 0.32D_o$ to be the most probable center-to-center separation of


DOI: 10.1021/jacs.5b10549
J. Am. Chem. Soc. 2015, 137, 15308−15314

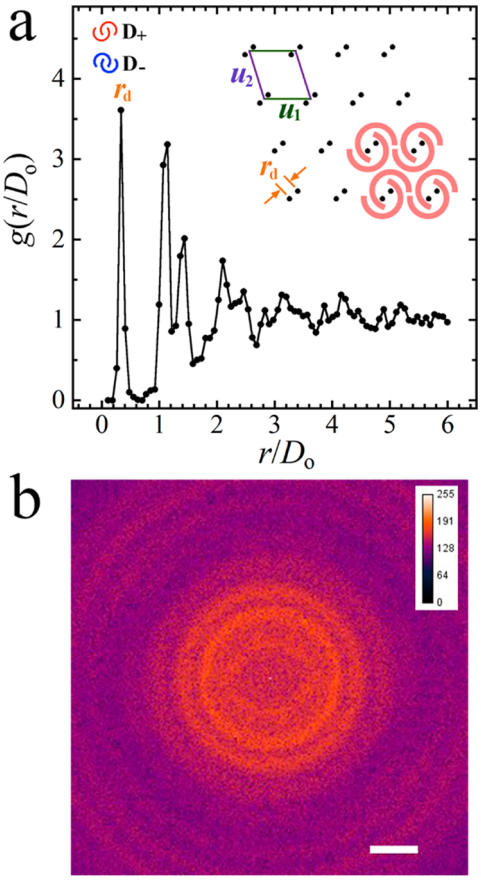


**Figure 4.** (a) Spatial pair correlation function $g(r/D_o)$ calculated from the dimer zone ($0\ \mu m \le z \le 88\ \mu m$) of the micrograph shown in Figure 1d. The center-to-center pair separation, $r$, is normalized by outer diameter, $D_o$, of the ASPs. The first dimer peak, located at $r_d/D_o \approx 0.32$, indicates the average center-to-center distance between ASPs in a dimer. The second and third peaks are related to the two unit vectors, $\mathbf{u}_1$ and $\mathbf{u}_2$, respectively, of an oblique local unit cell of dimers. Inset: oblique unit cell of a perfect $D_+$ dimer crystal. Each dimer is given by a pair of black dots (representing the centers of two ASPs) separated by $r_d$. (b) Fourier transform of the dense dimer region ($62\ \mu m \le x \le 152\ \mu m$, $0\ \mu m \le z \le 90\ \mu m$) of the micrograph shown in Figure 1d. White scale bar: 2 $\mu m^{-1}$. Inset (upper right): intensity scale of colors.

dimerized ASPs in that region. For larger separations, we find strong peaks at $r/D_o \approx 1.1$ and $r/D_o \approx 1.4$, corresponding to pairs of ASPs that are in nearest neighboring dimers. Other smaller peaks are found at larger $r/D_o$, but these only indicate short-range order, and overall the approach of $g$ toward unity indicates that the system is spatially disordered at long-range.

To explain the origin of the two local structural peaks in $g(r/D_o)$ beyond the dimer peak, we calculate $g(r/D_o)$ for a small idealized dimer crystallite composed of dimers having only a single chirality, based on nonoverlap of ASPs, where the equilibrium configuration is an oblique lattice pattern having two nonorthogonal basis vectors of lengths $|\mathbf{u}_1|$ and $|\mathbf{u}_2|$. Closely spaced pairs of dots correspond to dimers, and we draw $\mathbf{u}_1$ and $\mathbf{u}_2$ between the centers of these pairs (see Figure 4a: inset). By studying different interparticle distances within the dimer crystal, we conclude that the peak near $r/D_o \approx 1.1$ is related to packing of circles at a density, corresponding to the distance $u_1$, that is somewhat below close packing. Additional contributions to this peak come from shorter diagonals between ASPs in neighboring dimers in a 4-dimer local unit cell. The peak near $r/D_o \approx 1.4$ results from the longer diagonal distances between ASPs in the same 4-dimer local unit cell. Although randomness, created by the racemic mixture as well as monomer defects, in the experimentally observed dimer region destroys order at long-range, the crystal model is still useful in explaining the first few peaks beyond the dimer peak arising from local order in $g(r/D_o)$. The ring-like patterns that decay toward higher wavenumbers in the Fourier transform of the real-space monochrome micrograph ($62\ \mu m \le x \le 152\ \mu m$, $0\ \mu m \le z \le 90\ \mu m$) is also an indication of short-range order, as shown in Figure 4b. Some degree of azimuthal asymmetry is seen in the Fourier transform toward lower wavenumbers, indicating that there can be local orientational order between dimers composed of ASP monomers. This Fourier transform is interesting because it represents a combination of interference effects that would be seen in a scattering experiment from the experimentally observed system; this combination includes interference effects between interpenetrating ASPs within dimers as well as interference effects between dimers with other neighboring dimers. The separation of a Fourier transform into the product of a form factor of a single ASP and a structure factor,[30] which is appropriate for many molecular and colloidal systems, is not appropriate in this case because of the interpenetrating nature of the lock-and-key dimers.

## DISCUSSION

We have revealed nearly perfect subsurface dimerization of ASPs into a dense, spatially disordered state. This dense arrested dimer region lies below a reaction zone, where dimerization and dedimerization reactions are actively happening. This reaction zone, in turn, lies below a dilute, fluid-like surface layer of monomer ASPs. Since the ASPs have only hard interactions, the system's free energy is entirely determined by entropy and geometry, and the local arrangement of ASPs into dimers essentially is a byproduct of more efficient local organization that allows a larger number of translational and rotational microstates for all particles in the system. Thus, dimerization of hard ASPs by an applied osmotic pressure is different than well-known dimerization in systems of attractive monomers. It is interesting and striking that a form of local chiral symmetry breaking (LCSB)[22] occurs in each dimerization event, and the product dimers are found in racemic proportions, consistent with the achiral nature of individual ASPs. Dimers $D_+$ and $D_-$ are enantiomeric chiral objects, each having local unit cells with incommensurate edge lengths $|\mathbf{u}_1|$ and $|\mathbf{u}_2|$. Random (i.e. racemic) dimerization during the near-equilibrium slow compression of the system leads to spatial and orientational disorder over long-range even in the presence of Brownian fluctuations. Since there is some short-range orientational order among neighboring dimers, the system could be interpreted as being a polydomain liquid crystal[29] made up of very small domains, containing a scattering of monomer defects, the vast majority of which cannot easily recombine. Regardless of whether the system is regarded as a polydomain liquid crystal or a disordered glass, the dense racemic system of $D_+$ and $D_-$ is highly disordered at medium and long-range, and it exhibits nonergodic dynamics.

Although we have achieved a very high percentage of dimerization in the dense phase below the primary subsurface reaction zone, a few monomers, nearly all of which are isolated, still remain. Such isolated monomers are prevented from


DOI: 10.1021/jacs.5b10549
J. Am. Chem. Soc. 2015, 137, 15308−15314

diffusing into proximity of other monomers by the presence of many dimers in between. The probability of monomers moving by a series of successive dedimerization and redimerization events to finally recombine is also not entropically likely, since considerable local work must be done against the osmotic pressure for even a single dedimerization event to occur. In the reaction zone, it is possible for an odd number of ASPs in a local region to form as many dimers as possible, leaving only one ASP unpaired, simply as a consequence of the discrete nature of the building blocks. Since the reaction zone can be divided into many local regions, monomers in each region can be separated from each other, and their transport properties within the reaction zone relative to the rate of compression will largely control the density of residual isolated monomers found in the dense dimer region below. These monomers are effectively point-like defects trapped in the dense dimer region, although they can still rotate.

## CONCLUSION

In conclusion, we have performed experiments on Brownian systems of hard annular sector particles that reveal a high degree of dimerization. By investigating a very slow 2D osmotic compression of a Brownian monolayer of ASPs using optical microscopy, we have shown that the equilibrium constant $K$ of the dimerization reaction grows exponentially as $\Pi_{2D}$ increases. Moreover, we have revealed that the dense dimer region is predominantly composed of racemic populations of chiral enantiomers $D_+$ and $D_-$, a form of local chiral symmetry breaking that ultimately promotes disorder in the system. While individual ASPs are not bonded via attractive interaction into dimers, nevertheless, lock-and-key dimers of hard ASPs are well-defined, topologically identifiable structures, and these dimers can be treated as composite units according to principles of equilibrium thermodynamics governing composition and decomposition reactions.

Our exploration of this system of ASPs leads to a number of exciting future directions. Although we have demonstrated robust dimerization of a single ASP shape, a broader theoretical question still remains about how to generally describe all necessary characteristics of the entire range of shapes of hard particles that would give rise to robust dimerization, while excluding other potential local polymorphs, in a Brownian system subjected to a slowly applied osmotic pressure. It is possible that increasing the size of the reaction zone, for example by decreasing the tilt angle of the cuvette, could further reduce the already small monomer population in the dense dimer region. In addition, directly measuring the forward and reverse reaction rates in the reaction zone, by taking and analyzing time-lapse video recordings, could lead to a different alternative real-space method of determining $K$ for colloidal reactions through the principle of detailed balance. Finally, theoretically calculating the number of accessible microstates for ASPs or performing molecular or Brownian dynamics simulations at different densities could be used to predict the behavior that we have measured and generalize these results.

## AUTHOR INFORMATION

### Corresponding Author

*mason@chem.ucla.edu

### Notes

The authors declare no competing financial interest.

## ACKNOWLEDGMENTS

The authors thank M. Khan for discussions and the University of California-Los Angeles for financial support.

## REFERENCES

(1) Oxtoby, D. W.; Gillis, H. P.; Butler, L. J. *Principles of Modern Chemistry*, 8th ed.; Brooks Cole: Independence, KY, 2015.
(2) Bancroft, J. B.; Hills, G. J.; Markham, R. *Virology* **1967**, *31*, 354−379.
(3) Speir, J. A.; Munshi, S.; Wang, G.; Baker, T. S.; Johnson, J. E. *Structure* **1995**, *3*, 63−78.
(4) Asakura, S.; Oosawa, F. *J. Chem. Phys.* **1954**, *22*, 1255−1256.
(5) Asakura, S.; Oosawa, F. *J. Polym. Sci.* **1958**, *33*, 183−192.
(6) Mason, T. G. *Phys. Rev. E* **2002**, *66*, 060402.
(7) Zhao, K.; Mason, T. G. *Phys. Rev. Lett.* **2007**, *99*, 268301.
(8) Fujii, Y.; Yamada, H.; Mizuta, M. *J. Phys. Chem.* **1988**, *92*, 6768−6772.
(9) Branden, C.; Tooze, J. *Introduction to Protein Structure*, 2nd ed.; Garland Science: New York, 1999.
(10) Ohlendorf, D. H.; Anderson, W. F.; Lewis, M.; Pabo, C. O.; Matthews, B. W. *J. Mol. Biol.* **1983**, *169*, 757−769.
(11) Schevitz, R. W.; Otwinowski, Z.; Joachimiak, A.; Lawson, C. L.; Sigler, P. B. *Nature* **1985**, *317*, 782−786.
(12) Liu, Y.; Hart, P. J.; Schlunegger, M. P.; Eisenberg, D. *Proc. Natl. Acad. Sci. U. S. A.* **1998**, *95*, 3437−3442.
(13) Christie, J. M.; Arvai, A. S.; Baxter, K. J.; Heilmann, M.; Pratt, A. J.; O'Hara, A.; Kelly, S. M.; Hothorn, M.; Smith, B. O.; Hitomi, K.; Jenkins, G. I.; Getzoff, E. D. *Science* **2012**, *335*, 1492−1496.
(14) Ke, J.; Chen, R.-Z.; Ban, T.; Zhou, X. E.; Gu, X.; Tan, M. H. E.; Chen, C.; Kang, Y.; Brunzelle, J. S.; Zhu, J.-K.; Melcher, K.; Xu, H. E. *Nat. Struct. Mol. Biol.* **2013**, *20*, 1377−1382.
(15) Hernandez, C. J.; Mason, T. G. *J. Phys. Chem. C* **2007**, *111*, 4477−4480.
(16) Hoover, M. D.; Casalnuovo, S. A.; Lipowicz, P. J.; Yeh, H. C.; Hanson, R. W.; Hurd, A. J. *J. Aerosol Sci.* **1990**, *21*, 569−575.
(17) Brown, A. B. D.; Smith, C. G.; Rennie, A. R. *Phys. Rev. E* **2000**, *62*, 951−960.
(18) Sullivan, M.; Zhao, K.; Harrison, C.; Austin, R. H.; Megens, M.; Hollingsworth, A.; Russel, W. B.; Cheng, Z.; Mason, T. G.; Chaikin, P. M. *J. Phys.: Condens. Matter* **2003**, *15*, S11−S18.
(19) Zhao, K.; Mason, T. G. *Phys. Rev. Lett.* **2009**, *103*, 208302.
(20) Zhao, K.; Bruinsma, R.; Mason, T. G. *Proc. Natl. Acad. Sci. U. S. A.* **2011**, *108*, 2684−2687.
(21) Mayoral, K.; Mason, T. G. *Entropic Self-Organization of Tri-Star Colloids*; Electrum Publishing: Los Angeles, 2013 (ISBN 978-1939951-007).
(22) Zhao, K.; Bruinsma, R.; Mason, T. G. *Nat. Commun.* **2012**, *3*, 801.
(23) Zhao, K.; Mason, T. G. *J. Am. Chem. Soc.* **2012**, *134*, 18125−18131.
(24) Rossi, L.; Mason, T. G. *Soft Matter* **2015**, *11*, 2461−2468.
(25) Zhao, K.; Mason, T. G. *Proc. Natl. Acad. Sci. U. S. A.* **2015**, *112*, 12063−12068.
(26) Zhao, K.; Mason, T. G. *J. Phys.: Condens. Matter* **2014**, *26*, 152101.
(27) Bronshtein, I. N.; Semendyayev, K. A.; Musiol, G.; Mühlig, H. *Handbook of Mathematics*, 5th ed.; Springer: Berlin, 2007.
(28) Widom, B. *Statistical Mechanics: A Concise Introduction for Chemists*; Cambridge University Press: Cambridge, 2002.
(29) Chaikin, P. M.; Lubensky, T. C. *Principles of Condensed Matter Physics*; Cambridge University Press: Cambridge, 1995.
(30) Roe, R.-J. *Methods of X-ray and Neutron Scattering in Polymer Science*; Oxford University Press: Oxford, 2000.



DOI: 10.1021/jacs.5b10549
*J. Am. Chem. Soc.* 2015, 137, 15308−15314